A First-Order Radiative Transfer Model for Microwave Radiometry of Forest Canopies at L-Band

Mehmet Kurum, *Member, IEEE*, Roger H. Lang, *Fellow, IEEE*, Peggy E. O'Neill, *Senior Member, IEEE*, Alicia T. Joseph, Thomas J. Jackson, *Fellow, IEEE*, and Michael H. Cosh

***Abstract*—In this study, a first-order radiative transfer (RT) model is developed to more accurately account for vegetation canopy scattering by modifying the basic $\tau-\omega$ model (the zero-order RT solution). In order to optimally utilize microwave radiometric data in soil moisture (SM) retrievals over vegetated landscapes, a quantitative understanding of the relationship between scattering mechanisms within vegetation canopies and the microwave brightness temperature is desirable. The first-order RT model is used to investigate this relationship and to perform a physical analysis of the scattered and emitted radiation from vegetated terrain. This model is based on an iterative solution (successive orders of scattering) of the RT equations up to the first order. This formulation adds a new scattering term to the $\tau-\omega$ model. The additional term represents emission by particles (vegetation components) in the vegetation layer and emission by the ground that is scattered once by particles in the layer. The model is tested against 1.4-GHz brightness temperature measurements acquired over deciduous trees by a truck-mounted microwave instrument system called ComRAD in 2007. The model predictions are in good agreement with the data, and they give quantitative understanding for the influence of first-order scattering within the canopy on the brightness temperature. The model results show that the scattering term is significant for trees and modifications are necessary to the $\tau-\omega$ model when applied to dense vegetation. Numerical simulations also indicate that the scattering term has a negligible dependence on SM and is mainly a function of the incidence angle and polarization of the microwave observation.**

***Index Terms*—Emission, microwave radiometry, scattering, soil, vegetation.**

Manuscript received June 7, 2010; revised September 10, 2010 and October 22, 2010; accepted October 30, 2010. Date of publication December 23, 2010; date of current version August 26, 2011. This work was supported by an appointment to the NASA Postdoctoral Program at the Goddard Space Flight Center administered by Oak Ridge Associated Universities through a contract with NASA.

M. Kurum and P. E. O'Neill are with the Hydrological Sciences Branch, Hydrospheric and Biospheric Sciences Laboratory, NASA Goddard Space Flight Center, Greenbelt, MD 20771 USA (e-mail: mehmet.kurum@nasa.gov; kurum@gwmail.gwu.edu; peggy.e.oneill@nasa.gov).

R. H. Lang is with the Department of Electrical and Computer Engineering, The George Washington University, Washington, DC 20052 USA (e-mail: lang@gwu.edu).

A. T. Joseph is with the Hydrological Sciences Branch, Hydrospheric and Biospheric Sciences Laboratory, NASA Goddard Space Flight Center, Greenbelt, MD 20771 USA, and also with the University of Maryland, College Park, MD 20742 USA (e-mail: Alicia.T.Joseph@nasa.gov).

T. J. Jackson and M. H. Cosh are with the Hydrology and Remote Sensing Laboratory, Agricultural Research Service, U.S. Department of Agriculture, Beltsville, MD 20705 USA (e-mail: tom.jackson@ars.usda.gov; Michael.Cosh@ars.usda.gov).

Color versions of one or more of the figures in this paper are available online at http://ieeexplore.ieee.org.

Digital Object Identifier 10.1109/TGRS.2010.2091139

I. Introduction

SOIL MOISTURE (SM) is recognized as an important component of the water, energy, and carbon cycles at the interface between the Earth's surface and atmosphere, yet it is difficult to measure globally using traditional *in situ* techniques. Several planned microwave space missions, most notably the European Space Agency's Soil Moisture and Ocean Salinity (SMOS) mission (launched in November 2009) and NASA's Soil Moisture Active and Passive (SMAP) mission (to be launched in 2014/2015), are focusing on obtaining accurate SM information over as much of the Earth's land surface as possible [1], [2]. However, current baseline retrieval algorithms for SMOS and candidate retrieval algorithms for SMAP are based on an easily implemented but theoretically simple zero-order radiative transfer (RT) approach called the $\tau-\omega$ (tau–omega) model [3]. The model includes components from the soil and vegetation, but vegetation scattering is not represented properly. This approach essentially places a limit on the density of the vegetation through which SM can be accurately retrieved.

Both SMOS and SMAP have mission requirements to retrieve volumetric SM (VSM) to an accuracy of 0.04 $\text{cm}^3 \cdot \text{cm}^{-3}$ through vegetation water content (VWC) of 5 $\text{kg} \cdot \text{m}^{-2}$. These missions are expected to meet their requirement for SM retrieval accuracy using the heritage $\tau-\omega$ model approach over approximately 65% of the Earth's land surface where the VWC does not exceed 5 $\text{kg} \cdot \text{m}^{-2}$. As the density of vegetation increases, sensitivity to the underlying SM begins to degrade significantly, and errors in the retrieved SM increase accordingly. The zero-order $\tau-\omega$ model also loses its validity when dense vegetation (i.e., forest, mature corn, etc.) includes scatterers, such as branches and trunks (or stalks in the case of corn), which are large with respect to the wavelength. Thus, knowledge of vegetation features at L-band (1–2 GHz) appears to be of great importance in order to optimally utilize microwave radiometric data in SM retrievals over vegetated landscapes. The purpose of this paper is to develop a first-order model that takes into account vegetation scattering more accurately and that allows us to perform a physical analysis of the scattered and emitted radiation from vegetated terrain.

In the presence of vegetation, the emission from soil is attenuated and scattered by the vegetation, while the vegetation contributes its own emission. The question of how to separate the soil component from radiometer data collected over vegetated landscapes has been the subject of many papers

[3]–[18]. In order to understand and interpret measured data, several theoretical emission models have been developed and successfully validated in many cases [5]–[8]. The common approach to simulate the brightness temperature of vegetation is the RT theory [19]–[22], which can treat single and multiple scattering in a medium consisting of random discrete scatterers uniformly located in the vegetation layer. The theory assumes independent scattering and then disregards coherent effects.

A model based on the RT theory and the matrix-doubling algorithm was implemented by Ferrazzoli and Guerriero [7] and validated with experimental data. It considers the multiple-scattering effects of the volume scattering and the interactions between layers in the vegetation canopy and the underlying ground surface. The various contributions are combined by means of the matrix-doubling algorithm [21] to yield the bistatic scattering coefficient of a forest canopy. The latter was finally used to simulate the emissivity, through the energy conservation law.

A physical model for vegetation canopies that generalizes the restrictions imposed by earlier models with regard to the canopy type, temperature profile, and sky radiation was developed by Karam [8]. The vegetation is modeled as a multilayer random medium above a rough surface. This multilayer model is based on an iterative solution of the RT equations by using albedo as a perturbation (small) parameter, and the brightness temperature is expanded in a power series in albedo. Explicit expressions for zero- and first-order solutions of the albedo expansion are obtained. The model was validated with experimental data acquired over corn and soybean crops and also used to simulate emission from a walnut canopy. The first-order solution in albedo is also shown to be equivalent to Peake's emissivity formula [23] for canopies having uniform physical temperature profiles [8].

The Peake's emissivity formula in conjunction with a single-scattering approximation [24], which is called distorted born approximation (DBA), was implemented by Saatchi *et al.* [5] and Chauhan *et al.* [6] for a variety of land covers such as grass and corn. The procedure for calculation of vegetation emission is accomplished by first calculating the bistatic scattering cross section for each type of scatterer and then using the DBA to calculate the specular albedo of the ground and the diffused albedo consisting of the scattering from the vegetation layer and the surface roughness. Once the albedos are determined, Peake's principle relating active and passive problems is used to determine the effective emissivity of the vegetation layer.

In this paper, a microwave radiometry model that considers first-order scattering at L-band will be developed and validated against experimental data. The model assumes that the vegetation canopy has a uniform temperature and the soil surface may be rough. It is based on an iterative solution of the RT equations by interpreting the scattering source function as a perturbation to the nonscattering RT equations. This perturbation technique is known as the method of "successive orders of scattering" [25], [26]. The results are substantially simplified at L-band by taking the first two terms of the expansion of the transport result. It provides explicit expression for first-order scattering and emission processes that occur within the canopy. This formulation adds a new scattering term to the $\tau-\omega$ model (the zero-order RT solution). The additional term represents single scattered radiation by particles in the vegetation layer due to the emission generated by the ground and the particles in the vegetation layer. The resulting model represents an improvement over the standard zero-order solution since it accounts for the scattered vegetation and ground radiation that can have a pronounced effect on the observed emission and subsequent SM retrieval.

In Section II of this paper, the problem of RT through a discrete sparse medium is formulated by means of an iterative approach. In Section III, explicit expressions for zero- and first-order solutions of the successive orders of scattering expansion are obtained, and scattering properties of tree stands are also discussed. In Section IV, descriptions of instrumentation and the field experiment along with ground-truth data are given. In Section V, the zero- and first-order scattering solutions are compared with microwave brightness temperature data acquired over deciduous tree canopies in Maryland during 2007. Contributions of the individual scattering terms to the tree scattering are demonstrated. Significant terms contributing to forest scattering are identified, and their dependence on incidence angle and SM is demonstrated. Finally, Section VI summarizes the work presented in this paper.

II. Basic Problem Formulation

The starting point for microwave remote sensing of SM through vegetation is often classical RT theory. The RT approach is a heuristic method based on the law of energy conservation. The RT approach starts with the RT equation that governs the transport of specific intensity through a scattering medium. Due to the independent scattering assumption, RT is inherently an incoherent theory; therefore, it supplies no phase information and neglects any coherence effect. Because of its simple and intuitive nature, the RT approach has found widespread use in problems of passive microwave remote sensing of SM under vegetation. Most microwave SM retrieval algorithms developed for use at low microwave frequencies such as L-band or 1.4 GHz are based on a zero-order RT approach usually referred to as the $\tau-\omega$ model, where vegetation effects are parameterized by tau (the vegetation opacity) and omega (the single-scattering albedo).

As previously mentioned, the applicability of the $\tau-\omega$ model to areas with a significant tree fraction is unknown, particularly given its neglect of large scattering effects. It is likely that this approach will need modification (in terms of form or effective parameterization) to more accurately account for canopy scattering. The fundamentals of the RT theory offer one possibility on how to modify the $\tau-\omega$ model. The tree canopy can be envisioned as a random collection of discrete scatterers. Assuming that the average phase functions of tree components are known, together with their average forward-scattering cross sections, the RT equations can be formulated. The RT equations can then be solved iteratively up to the first-order scattering for a tree canopy since L-band is sufficiently low frequency and only single scattering will be important.

Fig. 1 shows an illustration of the forest model that will be employed here. The forested terrain is considered as a random

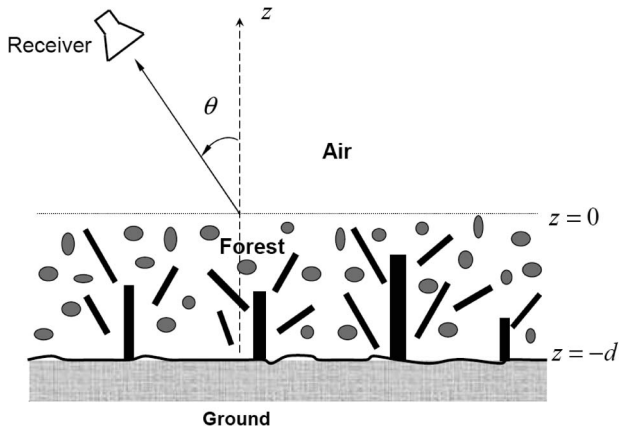

Fig. 1. Emission from a forest canopy over a rough ground.

medium of discrete lossy dielectric particles that are uniformly distributed between a ground plane at $z = -d$ and a diffuse upper boundary at $z = 0$, where d is the canopy layer thickness. The canopy is assumed to be over a homogenous dielectric half-space with a relative dielectric constant ε_g, representing the ground, and the interface between the ground and canopy is allowed to be rough. The vegetation layer will be represented as an ensemble of discrete scatterers with their orientation, size, and position statistics in a free-space background. It is assumed that scatterers of different kinds are uniformly located within the vegetation layer. The vegetation components have canonical shapes. The leaves are modeled as thin dielectric disks [27], [28]. Branches and trunks are modeled as finite-length dielectric cylinders of commensurate dimensions [29], [30]. The single-scattering characteristics of these constituents when averaged determine the attenuation and scattering properties of the canopy. The advantage of the discrete approach is that the results are expressed in terms of quantities (plant geometry and orientation statistics) that are related to the biophysical properties of individual plants.

For most of the vegetated terrain, it can be assumed that the orientation statistics for all scatterers are invariant in the azimuth coordinates. The specific intensity is thus only a function of the observation angle θ, and the solutions of RT equations are greatly simplified. It can also be shown that the third and fourth Stokes parameters are zero due to azimuthal rotational symmetry [20]. As a result, the vector transport equations can be written as two scalar equations, one for each polarization. The RT equations for up- and downwelling intensities are given, respectively, by

$$\cos\theta \frac{d}{dz} I_p(\theta, z) = -\kappa_{ep}(\theta) I_p(\theta, z) + \kappa_{ap}(\theta) C T_v + S_p(\theta, z) \tag{1.a}$$

$$-\cos\theta \frac{d}{dz} I_p(\pi - \theta, z) = -\kappa_{ep}(\pi - \theta) I_p(\pi - \theta, z) + \kappa_{ap}(\pi - \theta) C T_v + S_p(\pi - \theta, z) \tag{1.b}$$

where $I_p(\theta, z)$ and $I_p(\pi - \theta, z)$ are the upward and downward Stokes intensities for $0 \le \theta \le \pi/2$, respectively, including both vertical (v) and horizontal (h) polarizations, i.e., $p \in \{\mathrm{h}, \mathrm{v}\}$. The quantities $\kappa_{ep}(\theta)$ and $\kappa_{ap}(\theta)$ are the volume extinction and absorption coefficients, respectively, for polarization p. The first term at the right-hand side of (1.a) and (1.b) is due to the loss in the layer, and the second term represents the thermal emission contribution by the layer, which is equated to the radiation absorbed by the layer assuming local thermal equilibrium. The ambient temperature of the canopy is assumed to be uniform and is given by T_v. The constant C is given by $C = K/\lambda_0^2$, where K is the Boltzmann constant and λ_0 is the free-space wavelength.

The emitted radiations experience the same amount of attenuation within the vegetation irrespective of whether they travel in the angle of θ direction or the angle of $\pi - \theta$ direction. This is due to the reciprocity property of the particles and the azimuthal invariance to the particle rotation. As a result of these symmetries, the following notations will be employed: $\kappa_{ep}(\theta) = \kappa_{ep}(\pi - \theta)$ and $\kappa_{ap}(\theta) = \kappa_{ap}(\pi - \theta)$. By means of the forward-scattering theorem, the average vegetation extinction coefficient can be written as

$$\kappa_{ep}(\theta) = \frac{4\pi}{k_0} \sum_{\alpha} \rho_\alpha \mathrm{Im} \left\{ \left\langle f_{fpp}^{(\alpha)} \right\rangle \right\} \tag{1.c}$$

where the number density of the scatterer type α is given by ρ_α and k_0 is the wavenumber, i.e., $k_0 = 2\pi f_0/c$, with f_0 being the frequency and c being the speed of propagation in free space. The angular brackets in this formula denote ensemble average over the angular and size statistics of particles. The leaves are represented by an average-size circular disk; hence, the averaging is done for orientation angles only. The trunks are vertical and have a typical size. No averaging is therefore performed on trunks. The branch data are divided into several groups, and each group has an average length and an average diameter. Orientation averaging is then performed on each branch group. Notice that, in this formula, $f_{fpp}^{(\alpha)}$ is the forward-scattering amplitude of the αth group of scatterers.

The last term at the right-hand side of (1.a) and (1.b) represents the scattering contribution by the layer. The upward and downward scattering source functions $S_p(\theta, z)$ and $S_p(\pi - \theta, z)$ couple the equations for h- and v-polarized intensities as well as upward and downward radiations, and they are given by

$$S_p(\theta, z) = \int_{2\pi} d\Omega' \sum_{q=\mathrm{h,v}} \{F_{pq}(\theta, \phi; \theta', \phi') I_q(\theta', z) + F_{pq}(\theta, \phi; \pi - \theta', \phi') I_q(\pi - \theta', z)\} \tag{1.d}$$

where the polarizations p and q can be horizontal (h) or vertical (v) and the summation over q accounts for the possible polarization combinations. A similar expression for $S_p(\pi - \theta, z)$ can also be written by replacing θ with $\pi - \theta$ in (1.d). The integration in (1.d) is performed over 2π in the upper hemisphere, where $d\Omega' = d\phi' d\theta' \sin\theta'$. The collective phase function per unit volume is given by

$$F_{pq}(\theta, \phi; \theta', \phi') = \sum_{\alpha} \rho_\alpha \left\langle \left| f_{pq}^{(\alpha)}(\theta, \phi; \theta', \phi') \right|^2 \right\rangle \tag{1.e}$$

where the quantity $f_{pq}^{(\alpha)}(\theta,\phi;\theta',\phi')$ is the bistatic scattering amplitude of the αth group of scatterers. This function describes the scattering properties from direction (θ',ϕ') into direction (θ,ϕ).

The differential RT equations given in (1.a) and (1.b) will next be converted into integral equations. First, multiplying (1.a) by $e^{\kappa_{ep}(\theta)z\sec\theta}$ and integrating this from $-d$ to z give

$$\begin{aligned} I_p(\theta,z) &= e^{-\kappa_{ep}(\theta)(z+d)\sec\theta} I_p(\theta,-d) \\ &\quad + CT_v\left[1-e^{-\kappa_{ep}(\theta)(d+z)\sec\theta}\right][1-\omega_p(\theta)] \\ &\quad + \sec\theta\int_{-d}^{z} dz' e^{\kappa_{ep}(\theta)(z'-z)\sec\theta} S_p(\theta,z'). \end{aligned} \tag{2.a}$$

Similarly, multiplying (1.b) by $e^{-\kappa_{ep}(\theta)z\sec\theta}$ and integrating this from z to zero give

$$\begin{aligned} I_p(\pi-\theta,z) &= e^{\kappa_{ep}(\theta)z\sec\theta} I_p(\pi-\theta,0) \\ &\quad + CT_v\left[1-e^{\kappa_{ep}(\theta)z\sec\theta}\right][1-\omega_p(\theta)] \\ &\quad + \sec\theta\int_{z}^{0} dz' e^{-\kappa_{ep}(\theta)(z'-z)\sec\theta} S_p(\pi-\theta,z') \end{aligned} \tag{2.b}$$

where the above formulas are written in terms of the composite scattering albedo, which is denoted by $\omega_p(\theta)$, by employing energy conservation. This is the albedo of the average scatterer in the canopy. It represents the fractional power scattered from the average particle. The composite scattering albedo is given by [20]

$$\omega_p(\theta) = 1-\frac{\kappa_{ap}(\theta)}{\kappa_{ep}(\theta)} = \int_{4\pi} d\Omega' \sum_{q=\mathrm{h,v}} F_{pq}(\theta,\phi;\theta',\phi')/\kappa_{ep}(\theta). \tag{2.c}$$

To cast the integral equations (2.a) and (2.b) into a form suitable for iterative solution, the applicable boundary conditions will be incorporated into these equations from which the zero- and first-order solutions are driven. The vegetation upper boundary is assumed to be diffuse, and there is no radiation (from the upper atmosphere and cosmic background) going into the vegetation layer, i.e., at $z=0$

$$I_p(\pi-\theta,0) = 0. \tag{3.a}$$

At the soil surface $(z=-d)$, part of the downwelling radiation is reflected by the surface, while the ground contributes its own emission. The upward emission at the ground surface is given by

$$I_p(\theta,-d) = R_{gp}(\theta) I_p(\pi-\theta,-d) + [1-R_{gp}(\theta)]\, CT_g \tag{3.b}$$

where R_{gp} and T_g are the ground reflectivity and ground temperature, respectively. The tree site considered in this paper (refer to Section IV-B) is composed of planted Paulownia trees, and the ground under trees was relatively smooth. The surface *rms* height was on the order of 0.5–1 cm, which was rather low compared to the wavelength at L-band. As a result, only coherent component of the roughness is important for this study, and diffuse component is neglected. It is also assumed that the rough surface under the forest follows Kirchhoff's approximation and has a Gaussian height distribution [31]; therefore, the reflectivity of the rough surface is expressed as

$$R_{gp}(\theta) = \Gamma_{gp}(\theta) e^{-h\cos^2\theta}, \qquad p\in\{\mathrm{h,v}\} \tag{3.c}$$

where $\Gamma_{gp}(\theta)$ is the p-polarized Fresnel reflectivity of the average dielectric surface and the roughness height parameter is given by $h=4\sigma^2k_0^2$, with σ being the surface *rms* height. In addition to roughness, one should also consider moist litter present on most of natural forest floors, which could alter surface reflectivity significantly as verified by recent theoretical and experimental studies [32]–[34]. In this paper, the litter layer will not be considered since the experiment site under investigation did not have litter layer.

Substituting the boundary condition (3.a) in (2.b), the downwelling intensity at z within the vegetation layer is found as

$$\begin{aligned} I_p(\pi-\theta,z) &= CT_v\left[1-e^{\kappa_{ep}(\theta)z\sec\theta}\right][1-\omega_p(\theta)] \\ &\quad + \sec\theta\int_{z}^{0} dz' e^{-\kappa_{ep}(\theta)(z'-z)\sec\theta} S_p(\pi-\theta,z') \end{aligned} \tag{4.a}$$

and substituting (4.a), evaluated at $z=-d$, into (2.a) with the second boundary condition (3.b) yields the upwelling intensity at z within the vegetation layer as

$$\begin{aligned} I_p(\theta,z) &= CT_v\left[1-e^{-\kappa_{ep}(\theta)(z+d)\sec\theta}\right][1-\omega_p(\theta)] \\ &\quad + CT_v e^{-\kappa_{ep}(\theta)(z+d)\sec\theta} R_{gp}(\theta) \\ &\quad \times\left[1-e^{-\kappa_{ep}(\theta)d\sec\theta}\right][1-\omega_p(\theta)] \\ &\quad + CT_g e^{-\kappa_{ep}(\theta)(z+d)\sec\theta}[1-R_{gp}(\theta)] \\ &\quad + \sec\theta\int_{-d}^{z} dz' e^{\kappa_{ep}(\theta)(z'-z)\sec\theta} S_p(\theta,z') \\ &\quad + \sec\theta e^{-\kappa_{ep}(\theta)(z+d)\sec\theta} R_{gp}(\theta) \\ &\quad \times\int_{-d}^{0} dz' e^{-\kappa_{ep}(\theta)(z'+d)\sec\theta} S_p(\pi-\theta,z'). \end{aligned} \tag{4.b}$$

Equations (4.a) and (4.b) are the starting equations for iteration. The objective of the problem is to solve for upward propagating intensity at $z=0$ iteratively and then transmit it into the medium above the canopy layer.

III. Successive Orders of Scattering

Iterative techniques to solve RT equations have been extensively applied to microwave remote sensing of the Earth for more than three decades. The classic books of this subject include those of Ishimaru [19], Tsang *et al.* [20], Ulaby *et al.* [21],

and Fung [22], in addition to Karam's article [8] published in 1997. Iterative solutions of RT equations are described for active and/or passive problems of random medium. The volume scattering coefficient is usually considered small in these works, and as a result, the first-order solutions for active and/or passive problems refer to a first-order solution in volume scattering coefficient.

In this section, a similar approach with a different choice of small parameter is adapted to compute forest emission. Basically, the scattering source function [given in (1.d)] is interpreted as a perturbation to the nonscattering RT equations as oppose to volume scattering coefficient. This perturbation technique is known as the method of "successive orders of scattering" [25], [26]. In this technique, the brightness temperature is expanded into a series in terms of scattering mechanisms and substituted in RT equations. Then, collecting terms to the same order, the resulting RT equations are solved sequentially to the higher orders. The procedure is as follows: The zero-order RT solution is found by solving the nonscattering RT equations. The first-order solution of the RT equation with respect to the scattering source function is obtained by using the zero-order RT brightness temperature as an exciting source. The first-order solution is then substituted in the RT equations, and the second-order solution is obtained. This process is repeated to obtain higher order solutions which capture higher order scattering processes. Higher order scattering terms are usually not considered at L-band, and the results are substantially simplified at L-band by taking only the first two terms of the expansion of the transport result.

A. Zero-Order Solution (the $\tau-\omega$ Model)

The zero-order solution represents the solution to the nonscattering RT equations, where scattering is largely ignored by setting the scattering source functions $S_p(\theta, z')$ and $S_p(\pi-\theta, z')$ in (4.a) and (4.b) to zero. In this approximation, the vegetation canopy is treated as an effective attenuating layer, and the resulting equations for the up- and downwelling intensities can be obtained as

$$\begin{aligned} I_p^{(0)}(\theta, z) = {} & CT_v\left[1-e^{-\kappa_{ep}(\theta)(z+d)\sec\theta}\right][1-\omega_p(\theta)] \\ & + CT_v e^{-\kappa_{ep}(\theta)(z+d)\sec\theta} R_{gp}(\theta) \\ & \times\left[1-e^{+\kappa_{ep}(\theta)d\sec\theta}\right][1-\omega_p(\theta)] \\ & + CT_g e^{-\kappa_{ep}(\theta)(z+d)\sec\theta}[1-R_{gp}(\theta)] \quad (5.a) \end{aligned}$$

$$I_p^{(0)}(\pi-\theta, z) = CT_v\left[1-e^{+\kappa_{ep}(\theta)z\sec\theta}\right][1-\omega_p(\theta)]. \quad (5.b)$$

By using the relation between brightness temperature and intensity, i.e., $T_{Bp}(\theta, z) = I_p(\theta, z)/C$, the brightness temperature observed above the canopy (at $z \geq 0$) can be written as

$$\begin{aligned} T_{Bp}^{(0)}(\theta) = {} & [1-\gamma_p(\theta)][1-\omega_p(\theta)]T_v \\ & + \gamma_p(\theta)R_{gp}(\theta)[1-\gamma_p(\theta)][1-\omega_p(\theta)]T_v \\ & + \gamma_p(\theta)[1-R_{gp}(\theta)]T_g. \quad (6.a) \end{aligned}$$

Here, $T_{Bp}^{(0)}(\theta)$ is the zero-order RT brightness temperature observed above the vegetation, R_{gp} is the microwave reflectivity given in (3.c), T_v and T_g are the physical temperatures of the vegetation and soil, $\omega_p(\theta)$ is the composite scattering albedo given in (2.c), and $\gamma_p(\theta)$ is the vegetation transmissivity which is parameterized as (Beer's law)

$$\gamma_p(\theta) = e^{-\tau_p(\theta)\sec\theta} \quad (6.b)$$

where $\tau_p(\theta) = \kappa_{ep}(\theta)d$ is the vegetation opacity or optical thickness and θ is the observation angle from nadir.

Equation (6.a) is known in the SM community as the $\tau-\omega$ model [3]. Each term represents upwelling emission from the layer, downwelling emission from the layer reflected from the ground, and ground surface emission attenuated by the vegetation layer, respectively. The effect of scattering on this solution can be seen easily by assuming that vegetation and ground temperature is the ambient temperature and regrouping (6.a) in terms of albedo as

$$\begin{aligned} e_p^{(0)}(\theta) = {} & T_{Bp}^{(0)}(\theta)/Tv \\ = {} & \left[1-\gamma_p^2(\theta)R_{gp}(\theta)\right] - \omega_p(\theta)\left[1+\gamma_p(\theta)R_{gp}(\theta)\right] \\ & \times[1-\gamma_p(\theta)] \quad (7) \end{aligned}$$

where the first term represents the no scattering solution (independent of scattering albedo) and is also equivalent to the zero-order solution of the albedo expansion for canopies having uniform physical temperature profiles [8], [9].

Often, the albedo has been assumed to be either zero or small under the assumption that the scattering contribution of low vegetation such as grasslands and many agricultural crops is negligible. Researchers have sometimes further simplified the $\tau-\omega$ model by setting albedo to zero and used the first term in (7) for SM retrieval under vegetation [4].

It should also be noted that the presence of scattering [the second term in (7)] induces darkening in the zero-order solution since scattering hinders the emission from reaching an observing radiometer. To investigate the effect of the albedos of the individual tree constituents (branches, trunks, and leaves) on the zero-order solution, the scattering albedos of the deciduous Paulownia tree components are calculated and plotted in Fig. 2. The tree characteristics given in Table I of Section IV-B are used to generate these plots. The left column of the figure shows the angular and polarization dependence of the single-scattering albedos for branches, trunks, and leaves from top to bottom, respectively. In the second column, the branch contribution, the branch and trunk collective contributions, and the contributions of all of the tree constituents to the albedo are plotted in finer scale from top to bottom, respectively. From these plots, the following are shown: 1) The trunk albedo is highly angular and polarization dependent; 2) the leaves have the lowest albedo; and 3) the branches are the dominant constituents that determine the composite scattering albedo. These results are in agreement with theoretical findings [35] and also in agreement with experimental observations [15].

The values of the branch albedos for both polarizations are within the range of 0.5–0.6. This large albedo of a tree canopy

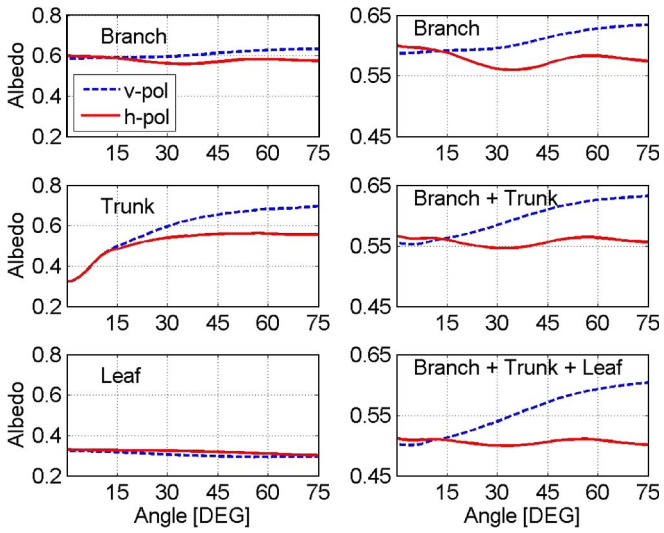

Fig. 2. Angular and polarization dependences of the individual and composite scattering albedos. The tree characteristics are provided in Table I of Section IV-B.

causes scatter-induced reduction in brightness temperature, and this scattering darkening effect for vegetation canopies (with large scatterers) should be balanced with a scattering contribution which is missing in (7). One solution to this problem is to adapt the formula given in (7) for forests with effective vegetation parameters tau and omega by fitting the experimental data or simulation outputs of a multiple-scattering model [35]. The effective albedo will not be the albedo of single forest elements anymore, but it becomes a global parameter, which depends on all the processes taking place within the canopy, including multiple scattering. In this paper, a different approach is applied to correct this scattering contribution to the zero-order solution by adding an extra term to (7), which will represent the first-order scattering term.

B. First-Order Solution

The term first order refers to a first-order scattering in scattering source function. The solution represents the single-scattering solution, i.e., the radiated emission from the layer or ground is scattered once by a scatterer. To find the first-order solution, RT equations need to be solved for upwelling intensity $I_p(\theta, z)$, and the solution will be evaluated at $z = 0$. The first-order specific intensity at the vegetation upper boundary is given by

$$I_p^{(1)}(\theta,0) = I_p^{(0)}(\theta,0) + \sec\theta \int_{-d}^{0} dz' e^{\kappa_{ep}(\theta) z' \sec\theta} S_p^{(0)}(\theta, z') + \sec\theta e^{-\kappa_{ep}(\theta) d \sec\theta} R_{gp}(\theta) \times \int_{-d}^{0} dz' e^{-\kappa_{ep}(\theta)(z'+d)\sec\theta} S_p^{(0)}(\pi-\theta, z') \quad (8)$$

where $S_p^{(0)}(\theta, z')$ and $S_p^{(0)}(\pi - \theta, z')$ represent the upward and downward scattering source functions, respectively, due to the zero-order emission. These quantities are obtained by substituting the zero-order scattering solutions (5.a) and (5.b) into the scattering source function given in (1.d). Carrying out the integrations in (8) over the canopy layer depth yields the following emissivity formulation:

$$e_p^{(1)}(\theta) = T_{Bp}^{(1)}(\theta)/T_v = e_p^{(0)}(\theta) + \Omega_p(\theta) \quad (9.a)$$

where the ambient temperatures of the vegetation layer and the ground are assumed to be the same, $e_p^{(0)}(\theta)$ is the zero-order solution as given in (7), and the parameter $\Omega_p(\theta)$ denotes the additional scattering term to the zero-order model, which represents the emission from the ground and the vegetation layer that is single scattered from tree trunks, branches, and leaves/needles in the case of forests and from thick stalks and leaves in the case of agricultural crops like corn. The scattering component $\Omega_p(\theta)$ is composed of eight terms representing different scattering mechanisms which are given by

$$\Omega_p(\theta) = \sum_j \left\{ \Omega_{jp}^{(s1)}(\theta) + \Omega_{jp}^{(sr1)}(\theta) \right\}, \quad \text{where } j \in \{G, U, D, DG\} \quad (9.b)$$

where the summation index j denotes the scattering-mechanism types, i.e., the subscripts G, U, D, and DG refer to the scattered radiation contributions due to ground emission, upwelling emission, downwelling emission, and downwelling emission followed by ground reflection, respectively. The processes of scattering are shown in Fig. 3. The scattered radiation from each mechanism arrives at the receiver either directly (denoted by $s1$) or through reflection from the ground (denoted by $sr1$) as shown in this figure. The explicit expressions for each scattering term are as follows.

1) Scattered Ground Emission: This term represents the ground emission that is scattered once from a particle in the layer as shown in Fig. 3(a). The scattered radiation arrives at the receiver either directly or through reflection from ground, and both received signals are given, respectively, by

$$\Omega_{Gp}^{(s1)}(\theta) = \sec\theta \int_{2\pi} d\Omega' \sum_{q=\mathrm{h,v}} F_{pq}(\theta,\phi;\theta',\phi') A_{1pq}(\theta,\theta') \times [1 - R_{gq}(\theta')] \quad (10.a)$$

$$\Omega_{Gp}^{(sr1)}(\theta) = \sec\theta R_{gp}(\theta)\gamma_p(\theta) \times \int_{2\pi} d\Omega' \sum_{q=\mathrm{h,v}} F_{pq}(\pi-\theta,\phi;\theta',\phi') \times A_{2pq}(\theta,\theta')\,[1 - R_{gq}(\theta')] \quad (10.b)$$

where the summation over q accounts for the possible polarization combinations and the integration over $d\Omega'$ accounts for all possible emitted radiation directions through which the emitted signal is scattered from the vegetation layer and propagates toward the receiver. The phase function $F_{pq}(\theta, \phi; \theta', \phi')$ is defined in (1.e), and it represents collective scattering from a unit volume within the vegetation layer. The quantities $A_{1pq}(\theta, \theta')$ and $A_{2pq}(\theta, \theta')$ in (10.a) and (10.b) are the result of the

TABLE I
CANOPY PARAMETERS FROM DESTRUCTIVE SAMPLING

TREE COMPONENTS	PARAMETERS				
	AVERAGE LENGTH [cm]	AVERAGE RADIUS [cm]	DENSITY [m^{-3}]	DIELECTRIC CONSTANT	ORIENTATION
TRUNKS	617.0	8.73	0.005	15.6+i3.8	*Vertical*
PRIMARY BRANCHES	187.0	4.30	0.016	12.0+i2.9	*Uniform [20°– 50°]*
	153.8	1.58	0.188	12.0+i2.9	*Uniform [10°– 60°]*
SECONDARY BRANCHES	63.6	0.98	0.734	12.0+i2.9	*Uniform [0°– 90°]*
	48.1	0.45	1.933	12.0+i2.9	*Uniform [0°– 90°]*
LEAVES	(AV. THICKNESS) 0.012	10.2	11.12	35.2+i5.3	*Uniform [0°– 90°]*

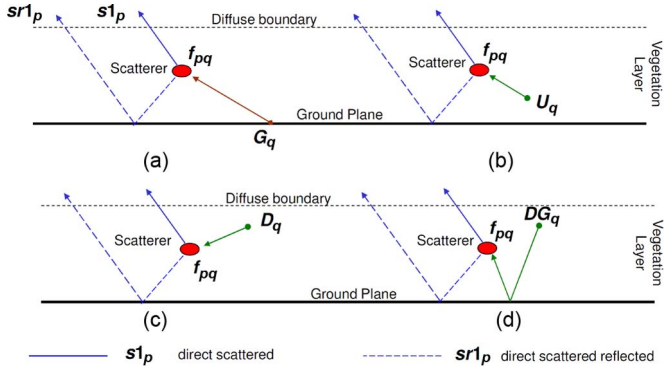

Fig. 3. First-order scattering mechanisms: (a) Scattered ground emission, (b) scattered upward emission from the vegetation layer, (c) scattered downward emission from the vegetation layer, and (d) scattered reflected-downward emission from the vegetation layer.

integration of the loss factors $e^{\kappa_{ep}(\theta)z\sec\theta}$ and $e^{\kappa_{eq}(\theta')z\sec\theta'}$ in various combinations associated with the unit volume located at z over the vegetation layer depth. These quantities are given by

$$A_{1pq}(\theta,\theta') = \frac{\gamma_q(\theta') - \gamma_p(\theta)}{\kappa_{ep}(\theta)\sec\theta - \kappa_{eq}(\theta')\sec\theta'} \tag{10.c}$$

$$A_{2pq}(\theta,\theta') = \frac{1 - \gamma_p(\theta)\gamma_q(\theta')}{\kappa_{ep}(\theta)\sec\theta + \kappa_{eq}(\theta')\sec\theta'} \tag{10.d}$$

where the volume vegetation extinction coefficient $\kappa_{ep}(\theta)$ and transmissivity $\gamma_p(\theta)$ are defined in (1.c) and (6.b), respectively.

2) Scattered Upward Emission From the Vegetation Layer: This term represents the upwelling emission that is scattered once from a particle in the layer as shown in Fig. 3(b). The scattered radiation arrives at the receiver either directly or through reflection from the ground, and both received signals are given, respectively, by

$$\Omega_{Up}^{(s1)}(\theta) = \sec\theta \int_{2\pi} d\Omega' \sum_{q=\mathrm{h,v}} F_{pq}(\theta,\phi;\theta',\phi') \times [A_{3p}(\theta) - A_{1pq}(\theta,\theta')]\,[1-\omega_q(\theta')] \tag{11.a}$$

$$\Omega_{Up}^{(sr1)}(\theta) = \sec\theta R_{gp}(\theta)\gamma_p(\theta) \int_{2\pi} d\Omega' \sum_{q=\mathrm{h,v}} F_{pq}(\pi-\theta,\phi;\theta',\phi') \times [A_{3p}(\theta) - A_{2pq}(\theta,\theta')]\,[1-\omega_q(\theta')] \tag{11.b}$$

where the quantity $A_{3p}(\theta)$ is the result of the integration of the loss factors $e^{\kappa_{ep}(\theta)z\sec\theta}$, associated with a unit volume located at z over the vegetation layer depth. This is given by

$$A_{3p}(\theta) = \frac{1-\gamma_p(\theta)}{\kappa_{ep}(\theta)\sec(\theta)}. \tag{11.c}$$

3) Scattered Downward Emission From the Vegetation Layer: This term represents the downwelling emission that is scattered once from a particle in the layer as shown in Fig. 3(c). The scattered radiation arrives at the receiver either directly or through reflection from the ground, and both received signals are given, respectively, by

$$\Omega_{Dp}^{(s1)}(\theta) = \sec\theta \int_{2\pi} d\Omega' \sum_{q=\mathrm{h,v}} F_{pq}(\theta,\phi;\pi-\theta',\phi') \times [A_{3p}(\theta) - A_{2pq}(\theta,\theta')]\,[1-\omega_q(\theta')] \tag{12.a}$$

$$\Omega_{Dp}^{(sr1)}(\theta) = \sec\theta R_{gp}(\theta)\gamma_p(\theta) \int_{2\pi} d\Omega' \sum_{q=\mathrm{h,v}} F_{pq}(\pi-\theta,\phi;\pi-\theta',\phi') \times [A_{3p}(\theta) - A_{1pq}(\theta,\theta')]\,[1-\omega_q(\theta')]. \tag{12.b}$$

4) Scattered Reflected-Downward Emission From the Vegetation Layer: This term represents the downwelling emission that is reflected from the ground and is followed by scattering once from a particle in the layer as shown in Fig. 3(d). The scattered radiation arrives at the receiver either directly or through reflection from the ground, and both received signals are given, respectively, by

$$\Omega_{DGp}^{(s1)}(\theta) = \sec\theta \int_{2\pi} d\Omega' \sum_{q=\mathrm{h,v}} F_{pq}(\theta,\phi;\theta',\phi') A_{1pq}(\theta,\theta') \times R_{gq}(\theta')\,[1-\gamma_q(\theta')]\,[1-\omega_q(\theta')] \tag{13.a}$$

$$\Omega_{DGp}^{(sr1)}(\theta) = \sec\theta R_{gp}(\theta)\gamma_p(\theta) \int_{2\pi} d\Omega' \sum_{q=\mathrm{h,v}} F_{pq}(\pi-\theta,\phi;\theta',\phi') \times A_{2pq}(\theta,\theta') R_{gq}(\theta')\,[1-\gamma_q(\theta')]\,[1-\omega_q(\theta')]. \tag{13.b}$$

Fig. 4. ComRAD microwave instrument system deployed over a stand of Paulownia trees.

IV. Instrumentation and Experiment

In this section, the experiment, along with the site information and the microwave instrument system used during the experiment, will be described. First, the ComRAD microwave active/passive instrument system is introduced with more emphasis on its L-band radiometer since this paper is concerned with passive data only. Then, the deciduous canopy and the associated ground truth are described.

A. Combined Radar/Radiometer System

The microwave instrument system used in this study is an outgrowth of a network-analyzer-based L-, C-, and X-band polarimetric radar system developed jointly by the NASA Goddard Space Flight Center and the George Washington University. The system is mounted on a 19-m hydraulic boom truck and has provided reliable calibrated radar data in SM field campaigns across the U.S. since the early 1990s. The truck system has been upgraded with the addition of a dual-polarized 1.4-GHz total power radiometer and is called ComRAD for combined radar/radiometer [36]. A novel broadband stacked-patch dual-polarized feed resonates at both the 1.4-GHz radiometer and 1.25-GHz radar frequencies, enabling both the L-band radar and radiometer to share the same 1.22-m parabolic dish antenna with 3-dB beamwidth of approximately 12°. The main purpose of this system is to provide microwave data for verifying the applicability of active and passive instruments in a combined manner for predicting the microwave emission from soils. A photograph of the truck system taking measurements over deciduous Paulownia trees is shown in Fig. 4.

ComRAD's L-band radiometer is a total power radiometer with a two-point internal calibration. The absolute accuracy and the sensitivity of the instrument are of ± 1 K and of ± 0.1 K, respectively. For internal calibration, the cold source is implemented by an amplifier with an isolator attached to the input and terminated by a 50-Ω matched microwave load, and the hot source is made up of a commercial hot noise source along with an attenuator. At an internal physical temperature of 45 °C, the reference hot sources are 401.2 K and 395.4 K for h- and v-polarized signals, respectively, and the cold sources are 154.5 K and 142.7 K for h- and v-polarized signals, respectively. The noise characteristics of the internal calibration sources were determined as a function of internal ambient temperature at the beginning of each field campaign. External calibration of the radiometer is carried out during each measurement run to correct the temperature variation and loss at the cables connecting the receiver and antenna. This external calibration is achieved using cold sky and ambient microwave absorber targets.

B. Experiment

In an effort to improve our understanding of the microwave properties of trees and their effect on SM retrieval algorithms, a coordinated sequence of field measurements involving the ComRAD active/passive microwave truck instrument system was initiated in late summer 2006. During fall 2006 (initial field checkout) and spring–fall 2007, ComRAD was deployed to a planted deciduous tree test site at an experimental farm run by the University of Maryland's Central Maryland Research and Education Center (CMREC) near Upper Marlboro, Maryland [37]. This paper will concentrate on the radiometer data collected in 2007 over stands of deciduous trees under no-leaf (April 10 and 25) and full-canopy conditions (May 18 and 24) as shown in Fig. 5. Supporting ground-truth data (including SM, ambient temperature, tree characteristics, etc.) were also collected during experiments. The total amounts of rainfall in the months of April and May for the Upper Marlboro region were 118.6 mm (above normal) and 27.2 mm (very dry, about half of normal), respectively, and the mean air temperatures were 10.8 °C (below normal) and 18.9 °C (well above normal), respectively. No precipitation occurred during any of the microwave measurements.

The site at CMREC consisted of plots of planted stands of deciduous Paulownia trees, a fast-growing deciduous tree with broad leaves. The tree plot used in this paper had 92 trees in a 1089-m^2 area. The dry biomass was about 9 kg/m^2, while the woody volume and density were 185.8 m^3/ha and 477.6 kg/m^3, respectively. The diameter at breast height (DBH) ranged from 17 to 23 cm (average DBH = 19.4 cm). The tree heights were variable, on the order of 11–14 m (average height = 13 m). Radiometer data were acquired at the height of 19 m above the ground level with incidence angles of 15°, 25°, 35°, and 45° from nadir. The corresponding footprints on the ground at these angles were 16.5, 20.1, 27.4, and 43.2 m^2, respectively. On experiment days, data were collected over a time span of about 2 h mostly during early morning. During the radiometer measurements, the truck boom was rotated in a conical scan

(a)

(b)

Fig. 5. Paulownia trees during (a) no-leaf and (b) full-canopy conditions.

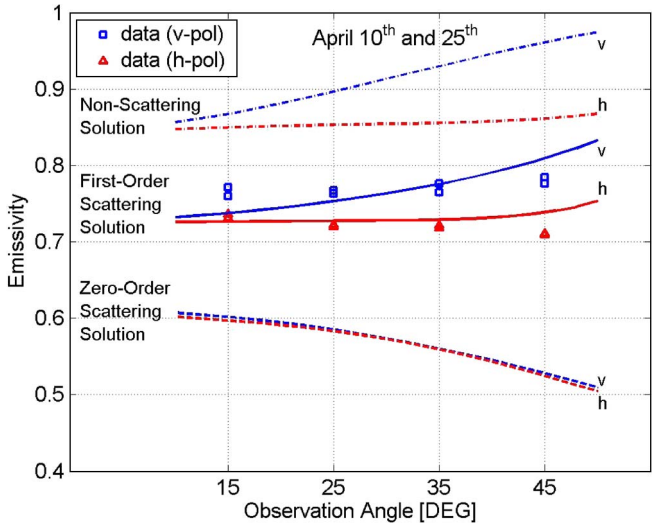

Fig. 6. Radiometric angular response from deciduous Paulownia trees is plotted. The dash-dot, solid, and dashed lines trace the simulated values of three models such as zero-order albedo, first-order scattering, and zero-order scattering solutions, respectively, while the squares and triangles represent v- and h-polarized measured data collected in April 2007, respectively.

arrangement at 15° increments within a 60° azimuth span. The resulting radiometer data for the tree plot at each incidence angle are an average of data from the three azimuthal observation locations.

Approximately coincident with the microwave measurements, theta probes which were inserted vertically into the first 6-cm depth of the soil and handheld infrared thermometers provided VSM and surface soil temperature, respectively. Ground measurements were taken at four arbitrary locations within each field of view and averaged for each incidence angle. Although the soil texture at the site was a loamy sand, consisting of 80% sand and 7% clay, the poor drainage features of the site resulted in generally wet soil conditions $(\mathrm{VSM} > 0.30\ \mathrm{cm}^3 \cdot \mathrm{cm}^{-3})$. The ground is flat with a relatively smooth surface, which consists of relatively short grass and weeds that were cut a few times during the year. The surface rms height was on the order of 0.5–1 cm, which was rather low compared to the wavelength at L-band.

The relative dielectric constants of the tree constituents were measured at L-band (1.25 GHz) *in situ* using dielectric probes connected to a vector network analyzer. The technique is based on reflection from an open-ended coaxial probe. The measured average relative dielectric constants are $35.2 + i5.3$ for leaves, $12.0 + i2.9$ for branches, and $15.6 + i3.8$ for trunks. To permit proper interpretation of the measured microwave signals, a representative tree outside the microwave footprint was cut down and destructively sampled. Detailed measurements of the size/angle distributions of the tree constituents (trunk, branches, and leaves), along with their densities, were made. The results from the canopy sampling and dielectric measurements are shown in Table I. The canopy sampling measurements were used in the model simulations described previously to produce emitted radiation at the ComRAD incidence angles so that simulation results can be compared with the measured data.

V. Results and Discussion

In this section, a set of canopy and surface parameters from the deciduous Paulownia stand is used to compute the response of the passive sensor. The goal is to use a physically based model such as the first-order RT approach to predict radiometric measurements and evaluate how the radiometer response to SM is modified by the forest canopy. The first-order scattering model will first be tested against the emissivity data (the ratio between the measured brightness and the ground ambient temperatures) from the deciduous Paulownia trees to verify the model validity by comparing with dual-polarization multiangular data collected in April. The model response to the seasonal and SM variations will then be evaluated. Once the model is validated, the effects of scattering are illustrated to indicate the model's major advantages. Illustrations are provided to show the contribution of each of the scattering processes described in Section III-B to the total received emission. The dependence of the scattering term on incidence angle and SM will also be explored at the end of this section.

The forest models described in Section III are used to calculate emissivity values at several incidence angles for the deciduous trees. To validate the first-order scattering model against the measured data and compare it with the nonscattering and zero-order scattering solutions, radiometric angular response from the deciduous trees is plotted in Fig. 6. In this figure, the nonscattering [the first term in (7)], the zero-order scattering

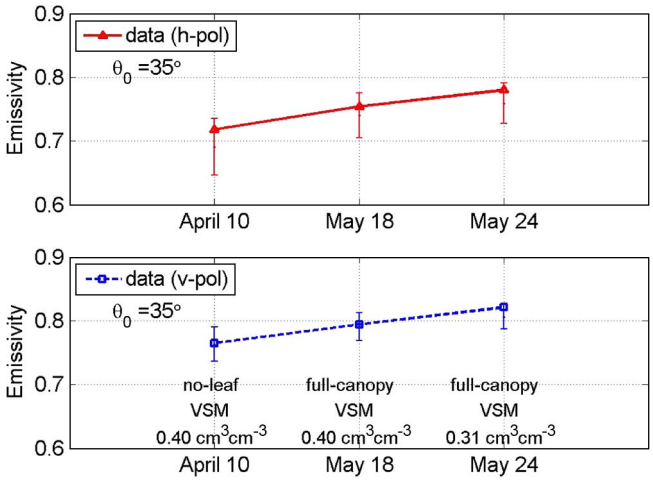

Fig. 7. Effect of season [April 10 (no leaf) versus May 18 (full canopy)] and SM [May 18 (VSM of 0.40 $cm^3 \cdot cm^{-3}$) versus May 24 (VSM of 0.31 $cm^3 \cdot cm^{-3}$) under full-canopy condition] at an observation angle of 35°. The upper plot shows h-polarization results, while the bottom plot shows v-polarization results. The error bars represent the simulated first-order model results for the range of surface *rms* heights of 0.5–1.0 cm.

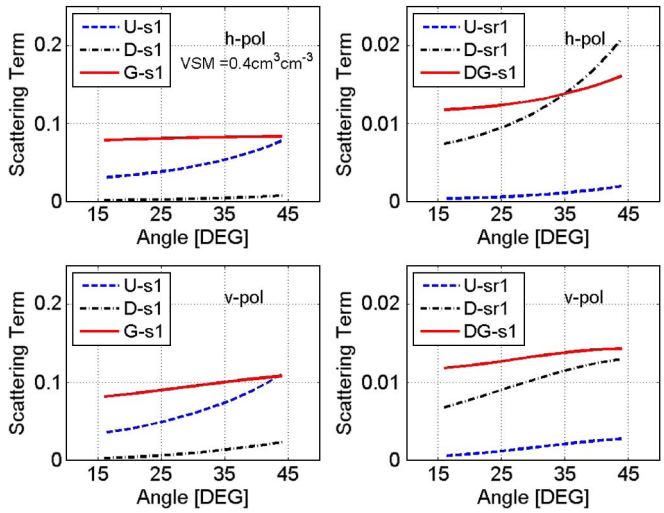

Fig. 8. Contributions of the individual scattering terms to the tree canopy scattering.

(the $\tau-\omega$ model), and the first-order scattering solutions are denoted by dash-dot, dotted, and solid curves, respectively. Soil with VSM of 0.38 $cm^3 \cdot cm^{-3}$ and a surface *rms* height equal to 0.9 cm was considered in the simulations. The square and triangles represent the measured data which were collected in April 10 (with VSM of 0.40 $cm^3 \cdot cm^{-3}$) and April 25 (with VSM of 0.36 $cm^3 \cdot cm^{-3}$) under no-leaf conditions. The mean air temperatures during microwave measurements for April 10 and 25 were 8 °C and 19 °C, respectively. As we see from the plot, the first-order solution captures the angular and polarization behavior of the data well, the $\tau-\omega$ model underestimates the tree emissivity for both polarizations, and the nonscattering solution overestimates the emissivity. The first-order solution balances the scattering albedo darkening effect with a single-scattering contribution for vegetation canopies (with large scatterers). The scattering in tree canopies takes place as a combination of reduction due to albedo and addition due to the single scattering.

In order to understand the impact of SM variations and foliation on the radiometric response, the measurements and the model generated curves for emissivity for three distinct days (April 10, May 18, and May 24) at an observation angle of 35° are plotted in Fig. 7. The solid line with triangular markers at the data points shows measured h-polarization, while the dashed line with square markers at the data points denotes measured v-polarization. The error bars represent the simulated first-order model results for the surface *rms* heights, σ, in the range of 0.5–1.0 cm, where the lower ends of the bars represent $\sigma = 0.5$ cm while the upper ends of the bars denote $\sigma = 1.0$ cm. In the figure, emissivities of full canopy (May 18) and no-leaf canopy (April 10) are compared, both of which had similar SM conditions (with VSM of 0.40 $cm^3 \cdot cm^{-3}$). Both model results and measured data for these dates show that the radiometer is able to resolve the change in tree state under the condition that the SM does not vary. It is observed that the emissivity increases as trees get foliated. This is due to the fact that the contribution of the tree emission to the total emission increases in the presence of leaves since the leaves have a significant effect on the canopy extinction and not much on scattering.

Fig. 7 also compares the effect of SM on the observed emissivity. The two days in proximity to each other (May 18 and May 24) were chosen to insure that the tree state did not change, but SM conditions were different. The mean air temperatures during microwave measurements for May 18 and 24 were 13 °C and 21 °C, respectively. As expected, the model predicts that emissivity increases with decreasing SM. This is due to the fact that emissivity of the ground increases with decreasing SM. A similar increase in measured emissivity is observed as the SM decreases from 0.40 $cm^3 \cdot cm^{-3}$ (May 18) to 0.31 $cm^3 \cdot cm^{-3}$ (May 24). For a fixed physical temperature of $T = 300$ K, the change in brightness temperature for a 0.09-$cm^3 \cdot cm^{-3}$ change in VSM is about 10 K. This clearly shows that the radiometer is able to sense SM variations under this type of tree canopy.

As a result of these model simulations and measurements given in Fig. 7, it can be concluded that both the soil surface and the tree canopy (SM and biomass) contribute together to the observed brightness temperature. Appropriate corrections for biomass must be made in order to make reliable SM estimation. In a similar manner, appropriate corrections for SM are needed to make reliable biomass estimation.

Fig. 8 shows significant terms contributing to the first-order scattering as a function of incidence angle. Note that the scale in plots on the right is given ten times finer than those on the left side for comparison purposes. The top figures represent h-polarization, while the bottom plots show results for v-polarization. The curve labels are defined in (9.b). As shown in the plots, the direct scattering terms for both polarizations due to upwelling (U-s1) and ground (G-s1) emissions are the most significant terms contributing to the first-order solution. The scattered upwelling (U-s1) emission is highly angular dependent, while the scattered ground (G-s1) emission is fairly constant over the range of angles plotted. Direct scattered downwelling (D-s1) emission is somewhat significant, and the reflected scattering (-sr1) terms are negligible compared to the direct scattered (-s1) terms.

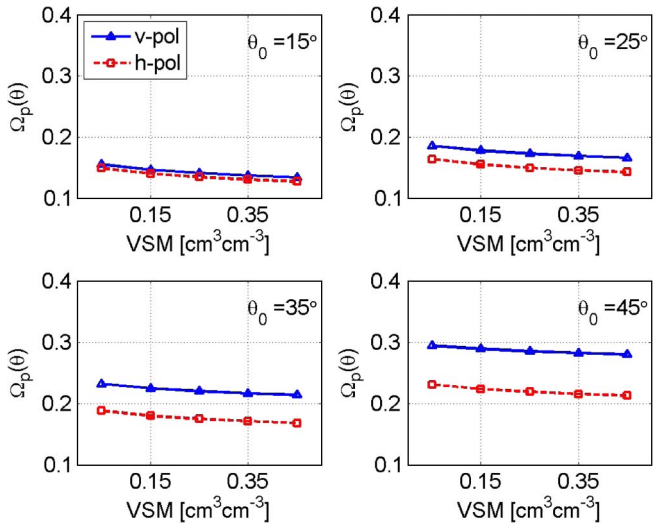

Fig. 9. Effect of SM on the total scattering term at the ComRAD observation angles (15°, 25°, 35°, and 45°).

In Fig. 9, the effect of SM on the total scattering term is shown. It shows the magnitude of the first-order scattering contribution over a range of VSM of 0.05–0.45 $\text{cm}^3 \cdot \text{cm}^{-3}$ at four different angles of observations. The plots indicate that the single scattered radiation increases the canopy brightness temperature considerably and it is mainly a function of the incidence angle and polarization of the microwave observation as also shown in Fig. 8. As the angle of observation increased from nadir, the scattering contribution increases and becomes more polarization dependent. This is because the v-polarized electric field becomes more aligned with the vertical tree components (vertical trunks and the tendency for the branches to be vertically oriented). The scattering term is complex since it is partly composed of single scattered energy that reflects from and is radiated by the soil surface. For typical values of SM as shown in the figure, the reflected scattering effect is negligible when compared to the direct scattering terms. This means that the scattering term is fairly constant over a wide range of SM conditions as confirmed by Fig. 9. This, in turn, can enable us to parameterize the scattering term with respect to specific vegetation types, anisotropic canopy structure, presence of leaves, and/or understory irrespective of the knowledge of moisture content of underlying soil.

VI. Summary and Conclusion

Despite the progress that has been made in the development of global SM retrieval algorithms, accurately correcting for the effects of vegetation scattering and attenuation over a wide range of vegetation canopies remains one of the ongoing challenges. In this paper, the development of a physically based model was pursued by employing a first-order vegetation scattering solution to RT equations. An analytical solution method of the RT equations, based on the successive orders of scattering, was described and used to calculate emission from forested terrain. The zero- and first-order scattering solutions were computed and compared with truck-based measurements of brightness temperature at L-band over small deciduous tree stands. It was found that the first-order scattering solution alone produces a good agreement with the experimental data. The first-order model was validated against multiangle deciduous data, and its response to seasonal and SM variations was also demonstrated. Contributions of the individual scattering terms to total tree scattering were discussed. Significant terms contributing to forest scattering were identified, and their dependence on incidence angle and SM was shown.

As the simulation results indicate, the $\tau-\omega$ model *will* need modification (in terms of form or effective parameterization) to enable accurate characterization of vegetation parameters when applied over moderately to densely vegetated landscapes. More scattering terms (at least up to first order at L-band) should be included in the RT solutions for forest canopies due to the large size of the tree canopy components with respect to wavelength. We propose a new SM retrieval model called the $\tau-\omega-\Omega$ model (the first-order RT model), given by

$$e_p^{(1)}(\theta) = \left[1-\gamma_p^2(\theta)R_{sp}(\theta)\right] - \omega_p(\theta)\left[1+\gamma_p(\theta)R_{sp}(\theta)\right]\left[1-\gamma_p(\theta)\right]+\Omega_p(\theta). \tag{14}$$

This model can be attractive for routine microwave SM retrieval since the formula relating terrain emission is physically based, takes canopy scattering into account properly, and requires few parameters. The new parameter $\Omega_p(\theta)$ depends on polarization and incidence angle and is mostly SM independent. This model could potentially overcome the vegetation scattering limitation and thus could be used with SMAP and SMOS data to increase the accuracy and reliability of SM products over moderately to densely vegetated landscapes. The implementation for this new SM inversion model is out of the scope of this paper and is left as future work.

References

[1] Y. H. Kerr, P. Waldteufel, J. P. Wigneron, S. Delwart, F. Cabot, J. Boutin, M. J. Escorihuela, J. Font, N. Reul, C. Gruhier, S. E. Juglea, M. R. Drinkwater, A. Hahne, M. Martin-Neira, and S. Mecklenburg, "The SMOS mission: New tool for monitoring key elements of the global water cycle," *Proc. IEEE*, vol. 98, no. 5, pp. 666–687, May 2010.

[2] D. Entekhabi, E. Njoku, P. E. O'Neill, K. Kellogg, W. Crow, W. Edelstein, J. Entin, S. Goodman, T. Jackson, J. Johnson, J. Kimball, J. Piepmeier, R. Koster, N. Martin, K. McDonald, M. Moghaddam, S. Moran, R. Reichle, J. C. Shi, M. Spencer, S. Thurman, L. Tsang, and V. Jakob, "The Soil Moisture Active and Passive (SMAP) mission," *Proc. IEEE*, vol. 98, no. 5, pp. 704–716, May 2010.

[3] T. Mo, B. Choudhury, T. Schmugge, J. Wang, and T. A. Jackson, "Model for microwave emission from vegetation covered fields," *J. Geophys. Res.*, vol. 87, no. C13, pp. 11 229–11 238, Dec. 1982.

[4] T. J. Jackson and T. J. Schmugge, "Vegetation effects on the microwave emission from soils," *Remote Sens. Environ.*, vol. 36, no. 3, pp. 203–212, Jun. 1991.

[5] S. S. Saatchi, D. M. Le Vine, and R. H. Lang, "Microwave backscatter and emission model for grass canopies," *IEEE Trans. Geosci. Remote Sens.*, vol. 32, no. 1, pp. 177–186, Jan. 1994.

[6] N. Chauhan, D. M. LeVine, and R. H. Lang, "Use of discrete scatter model to predict active and passive microwave sensor response to corn: Comparison of theory and data," *IEEE Trans. Geosci. Remote Sens.*, vol. 32, no. 2, pp. 416–426, Mar. 1994.

[7] P. Ferrazzoli and L. Guerriero, "Passive microwave remote sensing of forests: A model investigation," *IEEE Trans. Geosci. Remote Sens.*, vol. 34, no. 2, pp. 433–443, Mar. 1996.

[8] M. A. Karam, "A physical model for microwave radiometry of vegetation," *IEEE Trans. Geosci. Remote Sens.*, vol. 35, no. 4, pp. 1045–1058, Jul. 1997.

[9] R. H. Lang, C. Utku, P. de Matthaeis, N. Chauhan, and D. M. LeVine, "ESTAR and model brightness temperatures over forests: Effects of soil moisture," in *Proc. IEEE IGARSS*, Jul. 2001, vol. 3, pp. 1300–1302.
[10] G. Macelloni, S. Paloscia, P. Pampaloni, and R. Ruisi, "Airborne multifrequency L- to Ka-band radiometric measurements over forests," *IEEE Trans. Geosci. Remote Sens.*, vol. 39, no. 11, pp. 2507–2513, Nov. 2001.
[11] E. Njoku, E. Jackson, V. Lakshmi, T. Chan, and S. Nghiem, "Soil moisture retrieval from AMSR-E," *IEEE Trans. Geosci. Remote Sens.*, vol. 41, no. 2, pp. 215–229, Feb. 2003.
[12] R. H. Lang, C. Utku, P. E. O'Neill, and T. D. Tsegaye, "Role of albedo in sensing soil moisture under vegetation with passive L-band algorithms," in *Proc. IEEE IGARSS*, Sep. 2004, vol. 7, pp. 340–343.
[13] J. P. Wigneron, Y. H. Kerr, P. Waldteufel, K. Saleh, M. J. Escorihuela, P. Richaume, P. Ferrazzoli, P. de Rosnay, R. Gurney, J.-C. Calvet, J. P. Grant, M. Guglielmetti, B. Hornbuckle, C. Mätzler, T. Pellarin, and M. Schwank, "L-band Microwave Emission of the Biosphere (L-MEB) model: Description and calibration against experimental data sets over crop fields," *Remote Sens. Environ.*, vol. 107, no. 4, pp. 639–655, Apr. 2007.
[14] J. P. Grant, J. P. Wigneron, A. A. Van de Griend, A. Kruszewski, S. Schmidl Sobjerg, and N. Skou, "A field experiment on microwave forest radiometry: L-band signal behavior for varying conditions of surface wetness," *Remote Sens. Environ.*, vol. 109, no. 1, pp. 10–19, Jul. 2007.
[15] M. Guglielmetti, M. Schwank, C. Mätzler, C. Oberdorster, J. Vanderborght, and H. Fluhler, "Measured microwave radiative transfer properties of a deciduous forest canopy," *Remote Sens. Environ.*, vol. 109, no. 4, pp. 523–532, Aug. 2007.
[16] M. Guglielmetti, M. Schwank, C. Mätzler, C. Oberdorster, J. Vanderborght, and H. Fluhler, "FOSMEX: Forest Soil Moisture Experiments with microwave radiometry," *IEEE Trans. Geosci. Remote Sens.*, vol. 46, no. 3, pp. 727–735, Mar. 2008.
[17] E. Santi, S. Paloscia, P. Pampaloni, and S. Pettinato, "Ground-based microwave investigations of forest plots in Italy," *IEEE Trans. Geosci. Remote Sens.*, vol. 47, no. 9, pp. 3016–3025, Sep. 2009.
[18] A. Della Vecchia, P. Ferrazzoli, L. Guerriero, R. Rahmoune, S. Paloscia, S. Pettinato, and E. Santi, "Modeling the multifrequency emission of broadleaf forests and their components," *IEEE Trans. Geosci. Remote Sens.*, vol. 48, no. 1, pp. 260–272, Jan. 2010.
[19] A. Ishimaru, *Wave Propagation and Scattering in Random Media*. New York: Academic, 1978, ch. 7/8.
[20] L. Tsang, J. A. Kong, and R. T. Shin, *Theory of Microwave Remote Sensing*. New York: Wiley, 1985, ch. 3.
[21] F. T. Ulaby, R. K. Moore, and A. K. Fung, *Microwave Remote Sensing: Active, Passive Vol III: From Theory to Applications*. Dedham, MA: Artech House, 1986, ch. 13.
[22] A. K. Fung, *Microwave Scattering and Emission Models and Their Applications*. Norwood, MA: Artech House, 1994, ch. 3.
[23] W. Peake, "Interaction of electromagnetic waves with some natural surfaces," *IRE Trans. Antennas Propag.*, vol. 7, no. 5, pp. 324–329, Dec. 1959.
[24] R. H. Lang, "Electromagnetic backscattering from a random distribution of lossy dielectric scatterers," *Radio Sci.*, vol. 16, no. 1, pp. 15–30, Jan./Feb. 1981.
[25] J. Lenoble, Ed., *Radiative Transfer in Scattering and Absorbing Atmospheres: Standard Computational Procedures*. Hampton, VA: A. Deepak, 1985, pp. 46–48.
[26] J. Lenoble, M. Herman, J. L. Deuze, B. Lafrance, R. Santer, and D. Tanre, "A successive order of scattering code for solving the vector equation of transfer in the earth's atmosphere with aerosols," *J. Quant. Spectrosc. Radiat. Transf.*, vol. 107, no. 3, pp. 479–507, Oct. 2007.
[27] D. M. LeVine, R. Meneghini, R. H. Lang, and S. S. Seker, "Scattering from arbitrarily oriented dielectric disks in the physical optics regime," *J. Opt. Soc. Amer.*, vol. 73, no. 10, pp. 1255–1262, Oct. 1983.
[28] D. M. LeVine, A. Schneider, R. H. Lang, and H. G. Carter, "Scattering from thin dielectric disks," *IEEE Trans. Antennas Propag.*, vol. AP-33, no. 12, pp. 1410–1413, Dec. 1985.
[29] S. S. Seker and A. Schneider, "Electromagnetic scattering from a dielectric cylinder of finite length," *IEEE Trans. Antennas Propag.*, vol. 36, no. 2, pp. 303–307, Feb. 1988.
[30] M. A. Karam, A. Fung, and Y. Antar, "Electromagnetic wave scattering from some vegetation samples," *IEEE Trans. Geosci. Remote Sens.*, vol. 26, no. 6, pp. 799–808, Nov. 1988.
[31] B. J. Choudhury, T. J. Schmugge, R. W. Newton, and A. Chang, "Effect of surface roughness on the microwave emission from soils," *J. Geophys. Res.*, vol. 84, no. C9, pp. 5699–5706, Sep. 1979.
[32] A. Della Vecchia, P. Ferrazzoli, J. P. Wigneron, and J. P. Grant, "Modeling forest emissivity at L-band and a comparison with multitemporal measurements," *IEEE Geosci. Remote Sens. Lett.*, vol. 4, no. 4, pp. 508–512, Oct. 2007.
[33] M. Schwank, M. Guglielmetti, C. Mätzler, and H. Fluhler, "Testing a new model for the L-band radiation of moist leaf litter," *IEEE Trans. Geosci. Remote Sens.*, vol. 46, no. 7, pp. 1982–1994, Jun. 2008.
[34] J. P. Grant, A. A. Van de Griend, M. Schwank, and J. P. Wigneron, "Observations and modeling of a pine forest floor at L-band," *IEEE Trans. Geosci. Remote Sens.*, vol. 47, no. 7, pp. 2024–2034, Jul. 2009.
[35] P. Ferrazolli, L. Guerriero, and J. P. Wigneron, "Simulating L-band emission of forests in view of future satellite applications," *IEEE Trans. Geosci. Remote Sens.*, vol. 40, no. 12, pp. 2700–2708, Dec. 2002.
[36] P. E. O'Neill, R. H. Lang, M. Kurum, K. R. Carver, and C. Utku, "Multi-sensor microwave remote sensing of NASA's Combined Radar/Radiometer (ComRAD) system," in *Proc. IEEE MicroRad*, San Juan, PR, Feb. 2006, pp. 50–54.
[37] P. E. O'Neill, R. H. Lang, M. Kurum, A. T. Joseph, T. J. Jackson, M. H. Cosh, and R. Nelson, "ComRAD active/passive microwave measurements of tree canopies," in *Proc. IEEE IGARSS*, Barcelona, Spain, Jul. 2007, pp. 1420–1423.

Mehmet Kurum (S'08–M'09) received the B.S. degree in electrical and electronics engineering from Boğaziçi Üniversitesi, Istanbul, Turkey, in 2003 and the M.S. and Ph.D. degrees in electrical engineering from The George Washington University (GWU), Washington, DC, in 2005 and 2009, respectively.

During his graduate studies, he was a Research Assistant with GWU, where he conducted research in the radar time-domain characterization of wave propagation in forested landscapes, the development of the National Aeronautics and Space Administration (NASA)'s ComRAD system, the design of network-analyzer-based radar for NASA's 2-km microwave link, and the development of algorithms to measure rainfall over the link. Since 2009, he has been with the Hydrological Sciences Branch, Hydrospheric and Biospheric Sciences Laboratory, NASA Goddard Space Flight Center, Greenbelt, MD, where he conducts research in correcting the forest canopy effects on active/passive microwave remote sensing of soil moisture.

Roger H. Lang (F'89) received the B.S. and M.S. degrees in electrical engineering and the Ph.D. degree in electrophysics from the Polytechnic University, New York, NY, in 1962, 1964, and 1968, respectively.

From 1963 to 1964, he was with Bell Telephone Laboratories, where he worked on satellite antennas. From 1968 to 1970, he was with the Courant Institute of Mathematical Science, New York University, New York, where he did a postdoctoral work on wave propagation in random media. He is currently the T. Stanley Crane Professor of engineering and applied science with The George Washington University, Washington, DC. He is also currently the Chairman of the United States National Committee/International Union of Radio Science Commission F and a member of the editorial board of *Waves in Random and Complex Media*.

Peggy E. O'Neill (M'85–SM'03) received the B.S. degree (*summa cum laude*; with university honors) in geography from Northern Illinois University, DeKalb, in 1976 and the M.A. degree in geography from the University of California, Santa Barbara, in 1979.

She spent a year with Cornell University, Ithaca, NY, where she did a postgraduate work on civil and environmental engineering. Since 1980, she has been a Physical Scientist with the Hydrological Sciences Branch, Hydrospheric and Biospheric Sciences Laboratory, NASA Goddard Space Flight Center, Greenbelt, MD, where she conducts research in soil moisture retrieval and land surface hydrology, primarily through microwave remote sensing techniques. She is the Deputy Project Scientist for NASA's SMAP soil moisture mission.

Alicia T. Joseph received the B.S. degree in environmental science from Medgar Evers College, City University of New York, Brooklyn, in 1998, the M.S. degree in environmental and occupational health science from Hunter College, City University of New York, New York, in 2000, and the M.S. degree in geography and environmental engineering from The Johns Hopkins University, Baltimore, MD, in 2004. She is currently working toward the Ph.D. degree at the University of Maryland, College Park, with a research topic in "Physical and Semi-Empirical Approaches to Quantifying Microwave Optical Depth of Vegetation to Improve Estimates of Soil Moisture."

Since 2001, she has been with the Hydrological Sciences Branch, Hydrospheric and Biospheric Sciences Laboratory, NASA Goddard Space Flight Center, Greenbelt, MD, where she conducts research in the microwave remote sensing of soil moisture retrieval.

Thomas J. Jackson (A'86–M'96–F'02) received the Ph.D. degree from the University of Maryland, College Park, in 1976.

Since 1977, he has been with the Agricultural Research Service, U.S. Department of Agriculture, Beltsville, MD, where he is currently a Research Hydrologist with the Hydrology and Remote Sensing Laboratory. His research involves the application and development of remote sensing technology in hydrology and agriculture, primarily microwave measurement of soil moisture. He is or has been a Member of the science and validation teams of the Aqua, ADEOS-II, Radarsat, Oceansat-1, Envisat, ALOS, and SMOS remote sensing satellites.

Dr. Jackson is a Fellow of the American Meteorological Society and the American Geophysical Union. He is a member of the IEEE Geoscience and Remote Sensing Administrative Committee, where he serves as Secretary. He was the recipient of the AGU Hydrology Award in 2003. In 2003, he received the William T. Pecora Award (NASA and Department of Interior) for his outstanding contributions toward understanding the Earth by means of remote sensing.

Michael H. Cosh received the B.A. degree in engineering, with minors in math and physics, from Saint Francis College, Loretto, PA, in 1995, the B.S. degree (*magna cum laude*; with honors) in civil and environmental engineering from The Pennsylvania State University, University Park, in 1996, and the M.S. degree in hydraulics and hydrology and the Ph.D. degree in environmental fluid mechanics and hydrology from the School of Civil and Environmental Engineering, Cornell University, Ithaca, NY, in 1998 and 2002, respectively.

He is currently with the Hydrology and Remote Sensing Laboratory, Agricultural Research Service, U.S. Department of Agriculture, Beltsville, MD. His research interests include *in situ* soil moisture network validation, scaling of land surface parameters to satellite scale, and leaf wetness characterization and its interaction with microwave remote sensing.